



RESEARCH ARTICLE

10.1029/2023GC011024

Key Points:

- Bathymetric imaging reveals Kemp Caldera as a complex submarine caldera volcano with multiple collapse events
- New seafloor topography and visual data confirm hydrothermal venting at a central resurgent dome and along caldera margin
- Formation of the central resurgent cone by post-caldera dacitic magmatism

Correspondence to:

V. Kürzinger,
vkuerzinger@marum.de

Citation:

Kürzinger, V., Römer, M., Lichtschlag, A., & Bohrmann, G. (2023). Seafloor investigations of the Kemp Caldera, the southernmost arc caldera volcano from the South Sandwich island arc. *Geochemistry, Geophysics, Geosystems*, 24, e2023GC011024. <https://doi.org/10.1029/2023GC011024>

Received 27 APR 2023
Accepted 17 AUG 2023

Seafloor Investigations of the Kemp Caldera, the Southernmost Arc Caldera Volcano From the South Sandwich Island Arc

Victoria Kürzinger¹ , Miriam Römer^{1,2} , Anna Lichtschlag³, and Gerhard Bohrmann^{1,2} 

¹MARUM Center for Marine Environmental Sciences, University of Bremen, Bremen, Germany, ²Faculty of Geoscience, University of Bremen, Bremen, Germany, ³National Oceanography Centre, Southampton, UK

Abstract Kemp Caldera, situated in the south of the intra-oceanic South Sandwich arc, is one of the least explored submarine calderas that hosts hydrothermally active vent sites. The caldera was discovered in 2009. Since then, the focus has been primarily on biological studies. During the R/V *Polarstern* cruise PS119 in 2019, we gained new insights into the morphology, petrology and the formation of the Kemp Caldera. The ship's multibeam data provide an overview of the caldera bathymetry and backscatter characteristics. The new data revealed that the caldera is nested with two or possibly three concentric calderas. TV-sled and remotely operated vehicle (ROV) observations provide detailed visual data for the hydrothermally active sites of the vent field at the central resurgent cone and flare site at the NNW caldera rim. The central vent field is dominated by white smokers, where clams, sponges and other fauna thrive, while at the flare site inactive as well as actively venting chimneys have been found. The latter are characterized by metal-enriched fluids of temperatures $\geq 200^\circ\text{C}$. During ROV dives, rock samples were collected from the cone, providing the first information about the Kemp Caldera rock composition. The caldera rocks are dacitic, in contrast to the basalts and andesites of the neighboring Kemp Seamount. This suggests that the dacitic cone was formed by one or more later eruptions of differentiated magma, probably stored in shallow intrusions which are driving hydrothermal activity.

1. Introduction

Submarine hydrothermal activity is strongly related to tectonic settings, especially to active plate boundaries. Hydrothermal systems occur along mid-ocean ridges and volcanic arcs as well as in arc- and back-arc basins (e.g., de Ronde & Stucker, 2015; Peters et al., 2021). Heat exchange and fluid flow resulting from hydrothermal circulation are essential processes that influence the lithosphere and hydrosphere (Kleint et al., 2019; Seewald et al., 2015). Submarine calderas represent a special form of hydrothermal system. Large submerged arc caldera volcanoes within intra-oceanic arcs have gained increasing attention over the last few years. Hydrothermal venting hosted by these caldera volcanoes can lead to significant seafloor mineralization. Some mineralization types are rich in metals, for example, Fe, Cu, also Au, whereas other vents are dominated by only sulfur deposits (e.g., Berkenbosch et al., 2012; de Ronde et al., 2003, 2011; Kürzinger et al., 2022).

The development of marine technologies (including acoustic and towed camera systems, robots and geophysical methods) in the last decades has enabled the collection of samples of such seafloor mineralization as well as huge amounts of seafloor (bathymetric) data and mapping of large submarine areas. Multibeam and single beam echosounders are the most commonly used systems for seafloor mapping. The transmitted acoustic signals are processed to produce bathymetric maps, which enable structural and geological interpretations. The development of higher resolution bathymetric data provides more detailed information, allowing the identification of small-scale changes over time. Thus, seafloor mapping is not only applied as a tool to explore new areas but also to investigate known areas for changes over time.

Brothers and Niutahi in the SW Pacific are the only two hydrothermally active submarine arc caldera volcanoes which have been studied in more detail (in terms of fluid chemistry, seafloor mineralization, geochemistry and morphology; e.g., Berkenbosch et al., 2015; de Ronde et al., 2001, 2003, 2005). Another submarine caldera that hosts several hydrothermal sites is the Kemp Caldera, which is the largest submarine arc caldera volcano in the South Atlantic and one of the least explored submarine calderas. During the research cruise JR224 of the R/V *James Clark Ross* in 2009, new multibeam swath bathymetry data were collected. A highlight of the newly collected multibeam survey data was the discovery of the submarine Kemp Caldera west of Kemp Seamount

© 2023 The Authors. *Geochemistry, Geophysics, Geosystems* published by Wiley Periodicals LLC on behalf of American Geophysical Union. This is an open access article under the terms of the [Creative Commons Attribution-NonCommercial-NoDerivs License](https://creativecommons.org/licenses/by-nc-nd/4.0/), which permits use and distribution in any medium, provided the original work is properly cited, the use is non-commercial and no modifications or adaptations are made.

(Larter, 2009). Sites of hydrothermal activity in the Kemp Caldera (formerly known as “McIntosh Crater” or “McIntosh Caldera”) were observed during video footage taken on the JR224 cruise and the follow-up JC42 research cruise of the R/V *James Cook* in 2010 (C. S. Cole et al., 2014; Larter, 2009; Rogers, 2010). Note that, based on morphological criteria (e.g., aspect ratio, flat bottom, steep walls), Kemp Caldera was identified as a caldera and not a crater. Since its discovery, the Kemp Caldera has been intensively investigated from a biological point of view (see, e.g., Amon et al., 2013; Arango & Linse, 2015; Georgieva et al., 2015; Linse et al., 2019), but remains largely undescribed regarding its geological history and evolution. During the R/V *Polarstern* PS119 cruise in 2019, new bathymetry data along with visual seafloor observations and rock samples were collected and used to acquire information about the formation and evolution of the Kemp Caldera. This paper provides the first geological description of the caldera and the first petrological data for rock samples obtained from the caldera. Furthermore, backscatter data collected during the PS119 cruise give insights into Kemp Caldera surface characteristics, and TV-sled and remotely operated vehicle (ROV) dives enabled detailed descriptions of the hydrothermally active sites.

2. Geologic Setting

Kemp Caldera is a submarine arc caldera volcano located in the Scotia Sea and belongs to the southernmost part of the South Sandwich island arc. The Scotia Sea is enclosed by the Drake Passage to the west, the Weddell Sea to the south, and the Atlantic Ocean to the east and north. Directly beneath the Scotia Sea, the Scotia Plate and the smaller Sandwich micro-plate are situated (Figure 1a). The Scotia Plate boundary is marked by the North Scotia Ridge, East Scotia Ridge and South Scotia Ridge to the north, east and south, respectively. To the west, the plate is bounded by the Shackleton Fracture Zone. The extinct West Scotia Ridge spreading center in the western part of the Scotia Plate was active between 30 and 6 Ma ago, and was responsible for the formation of much of the oceanic lithosphere of the Scotia Plate (Riley et al., 2019). The intra-oceanic East Scotia Ridge, consisting of 10 ridge segments, represents not only the eastern boundary of the Scotia Plate but also the boundary of the Sandwich micro-plate to its west (James et al., 2014; Leat et al., 2000). Hydrothermal activity was recorded from the segments E2 in the north and E9 in the south (Figure 1a), from which hydrothermal vent fields such as “Dogs Head” and “Cindy’s Castle” are known (German et al., 2000; James et al., 2014; Rogers et al., 2012). Roughly 15 Ma ago, the East Scotia Ridge spreading started and has a current average spreading rate of ca. 65–70 mm/a (C. S. Cole et al., 2014; German et al., 2000). The crust is mainly made up of tholeiitic basalt and basaltic andesite (Fretzdorff et al., 2002; Leat et al., 2000).

The South Sandwich Trench represents the subduction zone to the east of the Sandwich micro-plate, where the plate overrides the subducting South American Plate (Leat et al., 2016; Livermore, 2003; Pearce et al., 2000). As a consequence of age difference, because older crust (~80 Ma) is subducted in the north than in the south (~27 Ma), the trench is much deeper in the north (>8 km) than in the southern part (<7 km) (Barry et al., 2006; Leat et al., 2004, 2010, 2016).

The formation of the South Sandwich island arc is also related to the subduction of the South American Plate under the Sandwich micro-plate. Due to the dehydration of the down-dipping slab, partial melting of the overlying mantle wedge is initiated, which leads to the formation of the South Sandwich Islands (Leat et al., 2003, 2013). In total, the South Sandwich island arc consists of 11 volcanic islands and numerous seamounts (Barry et al., 2006; Holdgate & Baker, 1979). The island’s lithology ranges from basalt to rhyolite and belongs to the (low-K) tholeiitic and calc-alkaline series (Barry et al., 2006; Larter et al., 1998; Leat et al., 2004). In addition to the East Scotia Ridge, hydrothermally active sites are also known from the island arc, in particular the Kemp Caldera in the south of the South Sandwich Islands (C. S. Cole et al., 2014; Larter, 2009). Thermal anomalies were also detected in the Quest Caldera in the northern part of the South Sandwich island arc (Linse et al., 2022). The Kemp Caldera belongs to the submerged part of the South Sandwich island arc and is located in the rear-arc ca. 25 km west of the main volcanic arc, represented by the Adventure Caldera (Figure 1b) (C. S. Cole et al., 2014; Kürzinger et al., 2022; Larter, 2009).

Most of the hydrothermal activity within the Kemp Caldera is known from the central area at the vent field (Figure 2a). Well-described features from the vent field include the Great Wall (Figure 4), which is a diffuse venting site named after a ca. one-m high wall-like structure consisting of weathered rock and covered by fine-crystalline sulfur as well as microbial mats (C. S. Cole et al., 2014; Hepburn, 2015; Kürzinger et al., 2022; Linse et al., 2019; Rogers, 2010). Toxic Castle and Winter Palace are white smoker vents located east of the Great

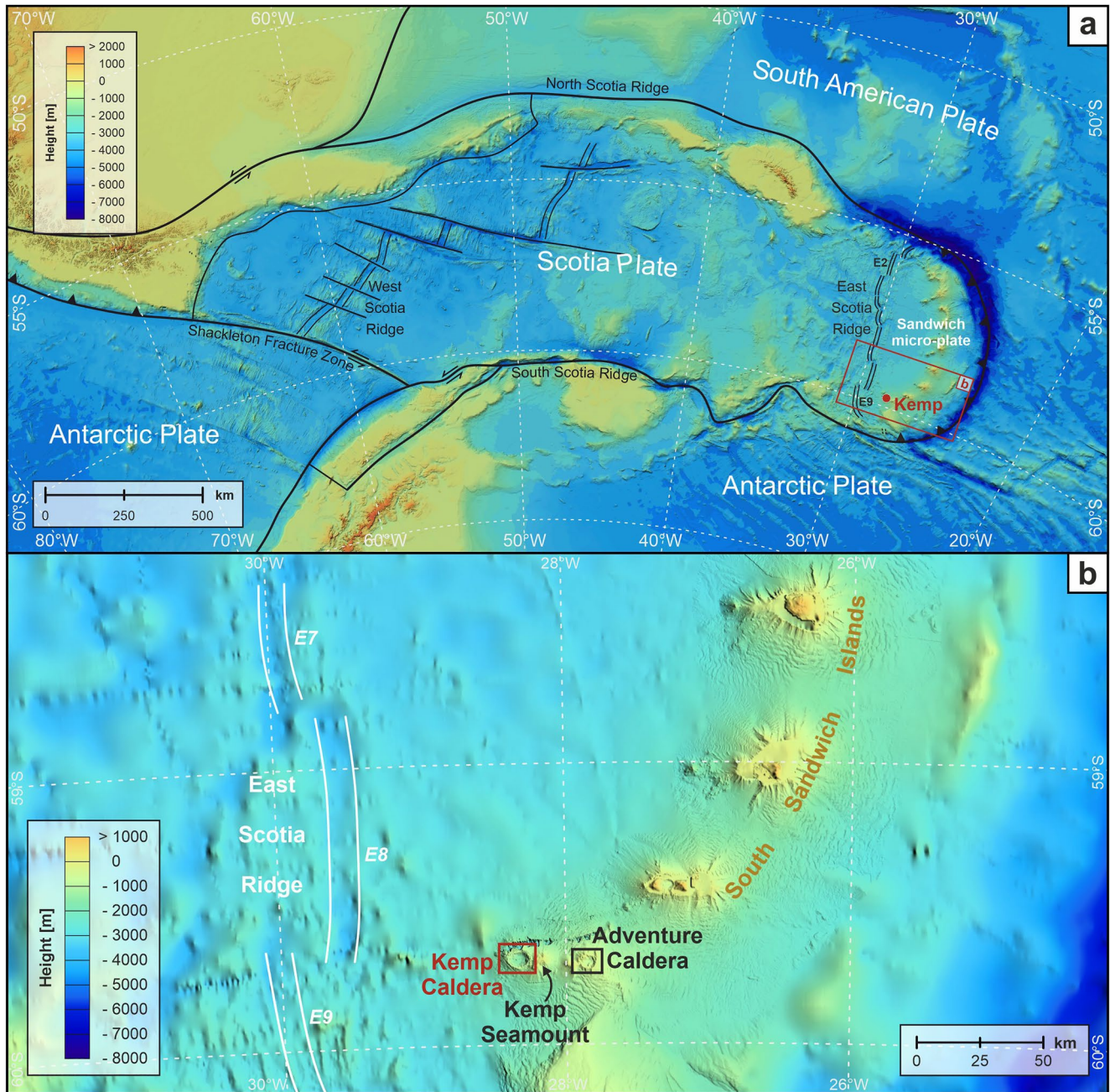


Figure 1. Bathymetric map of the Scotia Plate and its surroundings. (a) Important tectonic features of the Scotia Sea, Scotia Plate, and Sandwich micro-plate are shown on the map. The submarine Kemp Caldera (marked in red) is located in the south of the South Sandwich island arc on the Sandwich micro-plate. The area shown in (b) is marked in this map, (b) Bathymetric map of the southern part of the South Sandwich island arc showing the position of the Kemp Caldera within the line of volcanic islands. Kemp Caldera is located ~25 km west of the main volcanic arc next to Kemp Seamount and Adventure Caldera within the W–E line of volcanoes and seamounts.

Wall. Previously, Toxic Castle was known as a diffuse flow area (Hepburn, 2015; Tyler, 2011), but in 2019, it was found that the emitting fluids reached temperatures of more than 200°C, similar to those of Winter Palace (C. S. Cole et al., 2014; Kürzinger et al., 2022; Linse et al., 2019). An interesting phenomenon of Toxic Castle and Winter Palace is the occurrence of liquid sulfur, which partly covers the chimneys (Kürzinger et al., 2022; Rogers, 2010). Moreover, at Toxic Castle, a rather uncommon co-occurrence of sulfide minerals (e.g., covellite) and elemental sulfur (Kürzinger et al., 2022) has been described. The well-shaped covellite crystals are enclosed by a sulfur matrix.

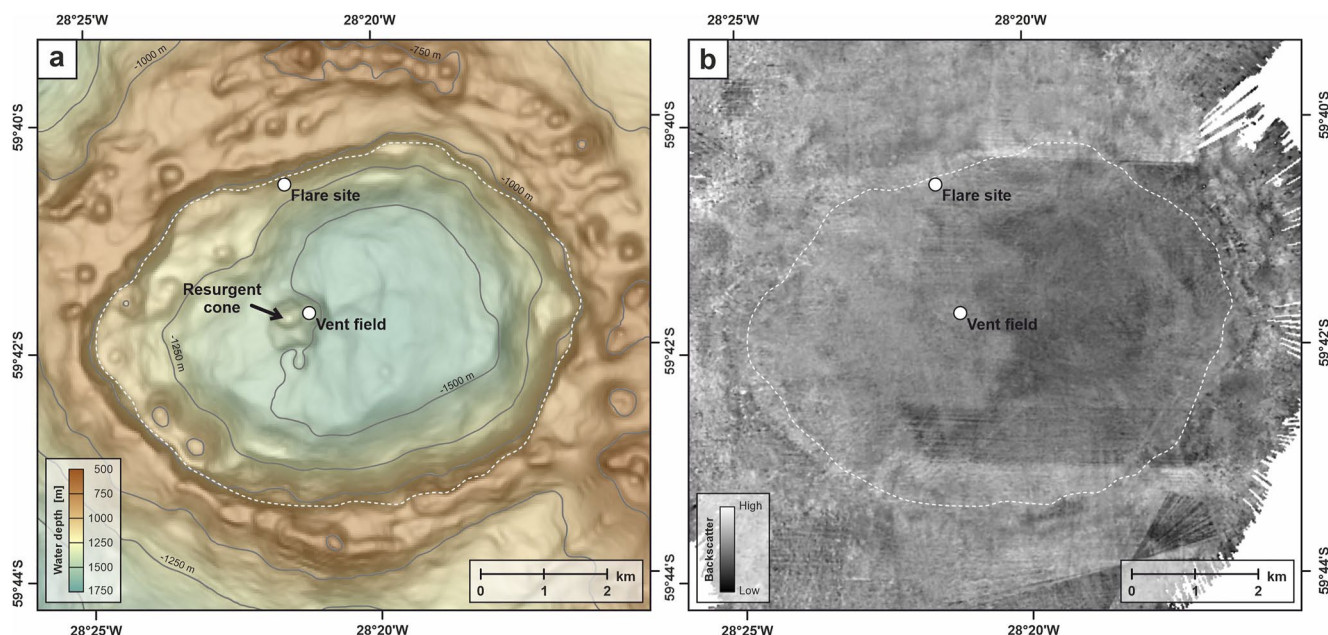


Figure 2. (a) Bathymetric map of the Kemp Caldera with the vent field (ca. 59°41.685'S, 28°21.015'W) and flare site (ca. 59°40.583'S, 28°21.433'W). The white dashed line indicates the upper edge of a stepped terrace at a water depth of ca. 1,070–1,170 m, and (b) Map of processed backscatter results.

A second hydrothermally active site was discovered during the R/V *Polarstern* PS119 expedition in 2019 (Bohrmann, 2019a, T. Pape, pers. comm.) at the NNW caldera rim (Figure 2a). Here, a bubble stream was detected in the water column as a hydroacoustic anomaly (also known as “flare”). During a visual seafloor survey at this flare site, an actively venting chimney was discovered and named Beehive Chimney; however, the gas bubble source could not be detected. The actively venting Beehive Chimney is characterized by fluid temperatures of ~230°C, and the relatively small chimneys (<20 cm) found there consist mainly of barite, chalcopyrite, marcasite, and sphalerite, showing a zonation pattern similar to that observed in other black smoker chimneys (Kürzinger et al., 2022).

3. Methods

During the R/V *Polarstern* PS119 research cruise in April/May 2019, multibeam and single beam swath bathymetry surveys were conducted at Kemp Caldera (Bohrmann, 2019a). For visual impressions and seafloor images, both a TV-sled named OFOBS (Ocean Floor Observation and Bathymetry System) and a ROV were used. In addition, rock samples were collected with the ROV (Table 1).

3.1. Hydroacoustic Data

Hydroacoustic data were collected during multibeam and single beam swath bathymetry surveys. Bathymetry and backscatter data were recorded with a hull-mounted *TELEDYNE HS-DS3* multibeam echosounder (MBES) at sounding frequencies between 14 and 17 kHz and applied for water depths of 30 to ca. 8,200 m. The collected data were post-processed using the open source MB-System software suite (Caress et al., 2017). The resulting grid displays high-quality seafloor data with a resolution of 30 m. Backscatter data were processed with CARIS

Table 1
Remotely Operated Vehicle (ROV) Dives Deployed at Vent Field for Visual Seafloor Mapping and Rock Sampling

Ship station	ROV dive	Latitude	Longitude	Water depth (m)	Sample ID	Description
PS119/028	ROV 447	59°41.679'	28°21.093'	1418.6	028-5R	Rock with fine-crystalline sulfur (Great Wall)
PS119/028	ROV 447	59°41.678'	28°21.095'	1416.7	028-6R	Rock from Great Wall
PS119/033	ROV 448	59°41.668'	28°21.054'	1427.2	033-3B	Rock from clam field

Hips&Sips. Sub-bottom profiler data were collected using a hull-mounted *TELEDYNE PARASOUND P70* echosounder. Visualization was done with IHS Kingdom Suite.

3.2. Ocean Floor Observation and Bathymetry System (OFOBS)

An OFOBS was deployed to acquire seafloor images. A complete list of all devices mounted at the OFOBS and its functionality is described in detail in Purser et al. (2019). In this study, the following devices were used: for visual seafloor observations, a high-resolution digital camera *iSiTEC, CANON EOS 5D Mark III*, equipped for still frames and a *Sony FCB-H11* HD color camera for video recording, and a Posidonia ultra-short baseline (USBL) transponder for underwater positioning. For the cleaning of outliers, smoothing and interpolation to 1 sec the software tool of Marcon (2019) was used.

3.3. The ROV *MARUM QUEST 4000*

The ROV *MARUM QUEST 4000* was deployed to collect additional seafloor images. To enhance the video imaging quality, two ultralow latency HDTV cameras, a 4k video tiling system, a stereo camera with corrected optics and a still camera prototype (15 Mpx) were installed on the vehicle. A Doppler Velocity Log (DVL, 1,200 kHz) was used to perform stationing, displacement and other automatic control functions.

Rock samples were collected from the caldera floor using the ROV (Table 1). With its hydraulic manipulator arm, the rock samples were collected (either with a shovel or with the claw of the manipulator arm), placed in the vehicle basket, and transported to the surface. For microscopic investigations, polished thin sections from the rock samples were prepared and examined in terms of mineral identification and texture of igneous rocks. For this purpose, a LEICA DMRX stereomicroscope was used. Additionally, X-ray fluorescence (XRF) analysis was used to determine the elemental composition of the rocks. The XRF analysis was conducted at the Institute for Chemistry and Biology of the Marine Environment (ICBM) in Oldenburg.

4. Results

4.1. Morphology and Backscatter

The main purpose of the multibeam swath bathymetry surveys was bathymetric mapping to gain new insights into the geomorphology of the Kemp Caldera (Figure 2).

In the bathymetric map, it is seen that the Kemp Caldera has a subcircular shape (Figure 2a). It has a rim-to-rim extension from north to south of about 6.5 km and an east-west width of roughly 8.6 km. At its deepest point in the eastern center, the caldera floor is ~1,618 m deep, while the western caldera floor is shallower and reaches a maximum depth of ca. 1,440 m. The caldera rim lies at a water depth of mainly between 800 and 900 m. Several secondary cones are found, especially at the northern and eastern caldera rims, which are generally between 20 and 50 m high, but some of them reach heights of up to 100 m. Their basal diameter is highly variable, ranging from a few tens of meters to several hundred meters. The biggest secondary cone is located north of the caldera and reaches a depth of about 610 m below the water surface. At the northern caldera rim, most of these cones have a conical shape with a rounded top, whereas in the east/southeast, small caldera structures occur. In the western center of the Kemp Caldera, there is also a secondary cone, interpreted as a resurgent cone (Kürzinger et al., 2022; Linse et al., 2019). The top of this cone lies at a water depth of about 1,339 m and thus towers over the caldera floor by more than 270 m. The top of this cone is rounded, and visual seafloor observations revealed that the resurgent cone has little to no sediment cover, exposing lavas at its surface. Measured from the shallower caldera floor to the west (water depth of ~1,440 m), the diameter of the resurgent cone at this base is between 680 m in the NW–SE direction and 860 m in the WSW–ENE direction. The slope angle of the flanks mainly varies between 17 and 24°. Inside the caldera at a depth of about 1,070 m in the west and about 1,170 m in the east close to the rim, a morphologic step can be seen as a stepped terrace at the inner caldera wall (Figure 2a). This step marks a change of slope angle of the caldera walls. The upper caldera wall, which is between ca. 170 and 370 m high, has a maximum slope angle of ca. 38° in the southwest and north (in places even up to 55°), while the lower part mainly shows slope angles between 10 and 20°.

Backscatter data were used to obtain an overview of the Kemp Caldera surface facies and the roughness of the seafloor. The distinction between high and low reflectance is represented as a brightness gradation: white (high reflectance, usually indicating harder or rougher surfaces) to black (low reflectance, usually indicating softer or smoother surfaces). As seen in Figure 2b, the Kemp Caldera floor shows a rather inhomogeneous

backscatter pattern. However, two different backscatter facies separate the caldera floor in an eastern and a western part of similar extent along a roughly N to S directed lineation. A lower backscatter appears to characterize the eastern part of the caldera floor, while the western part shows a relatively high backscatter, similar to the caldera rim.

4.2. OFOBS Seafloor Observations and Sub-Bottom Information

As mentioned above, there are two backscatter facies dividing the Kemp Caldera in the eastern and western parts. Based on OFOBS seafloor observations, the reasons for differences between the backscatter facies could be described in more detail. The area of low reflectance is characterized by sediment as soft ground (Figure 3d), while the western area is dominated by hard ground consisting of volcanic rock (Figure 3c), which reflects the signals of the ship-based multibeam echosounder in high intensity.

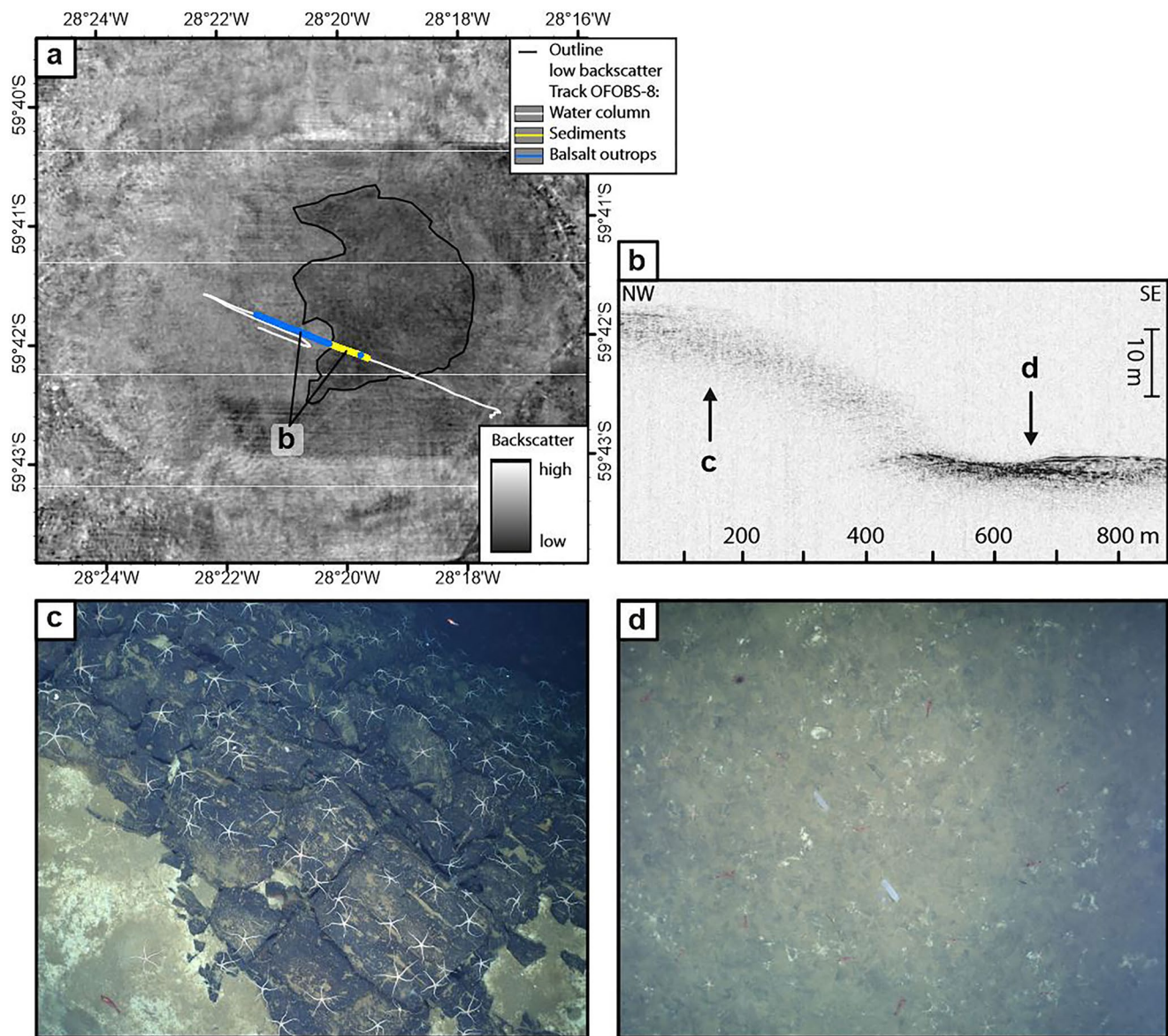


Figure 3. (a) Backscatter data (eastern part with lower reflectance is framed) with the OFOBS-8 track (white line). The blue and yellow highlighted line denotes the sub-bottom profile in (b), (b) Sub-bottom profile displaying the transition from the area of high reflectance (c) to the area of low reflectance (d), (c) Seafloor image showing a steep slope of blocky volcanic rock colonized by a large number of brittle stars, and (d) Sediment-covered area in the eastern half of the caldera.

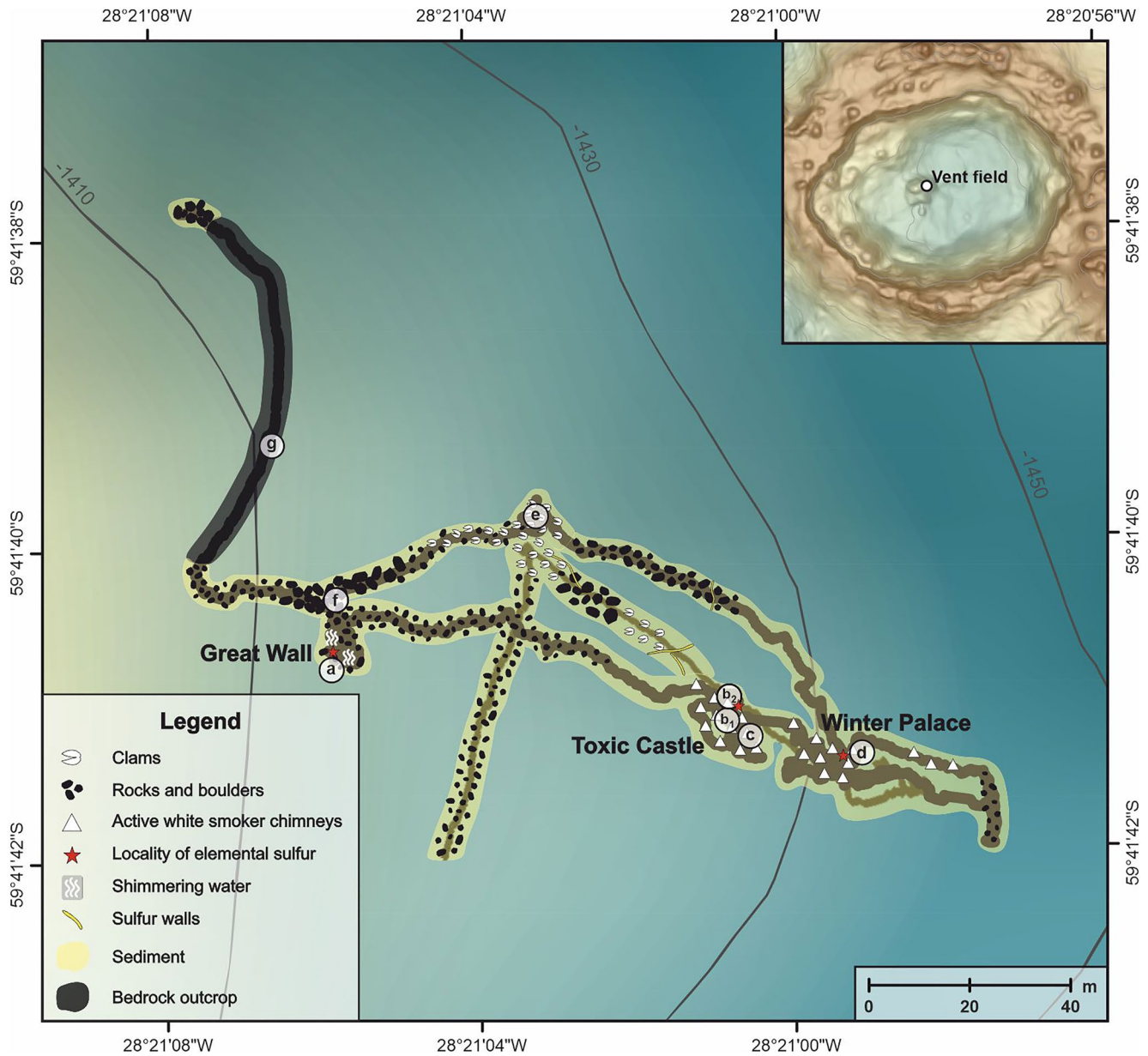


Figure 4. Map created from visual remotely operated vehicle (ROV) seafloor observations (ROV 447 and 448) of the vent field area. The letters in the map refer to the corresponding letters of seafloor images in Figure 5.

With respect to the sub-bottom information, imaging of subsurface structures could barely be displayed. This is due to a very steep caldera rim and little penetration at the western caldera part, caused by a rough and bumpy seafloor surface, resulting in scattering of the signal and a cloudy, almost transparent seafloor reflection. Only in the eastern part of the caldera, the penetration of a few meters into the sub-bottom was achieved and layers, which partly could be identified as sediment, were visible (Figure 3b).

4.3. Visual Seafloor Mapping

Using ROV video surveys, visual seafloor mapping was conducted in two hydrothermally active areas of the Kemp Caldera: (a) the vent field at the foot of the eastern flank of the resurgent cone in the caldera's center, and (b) the flare site at the NNW of the caldera (Figure 2a). Results of the visual mapping are summarized in Figures 4 and 6.

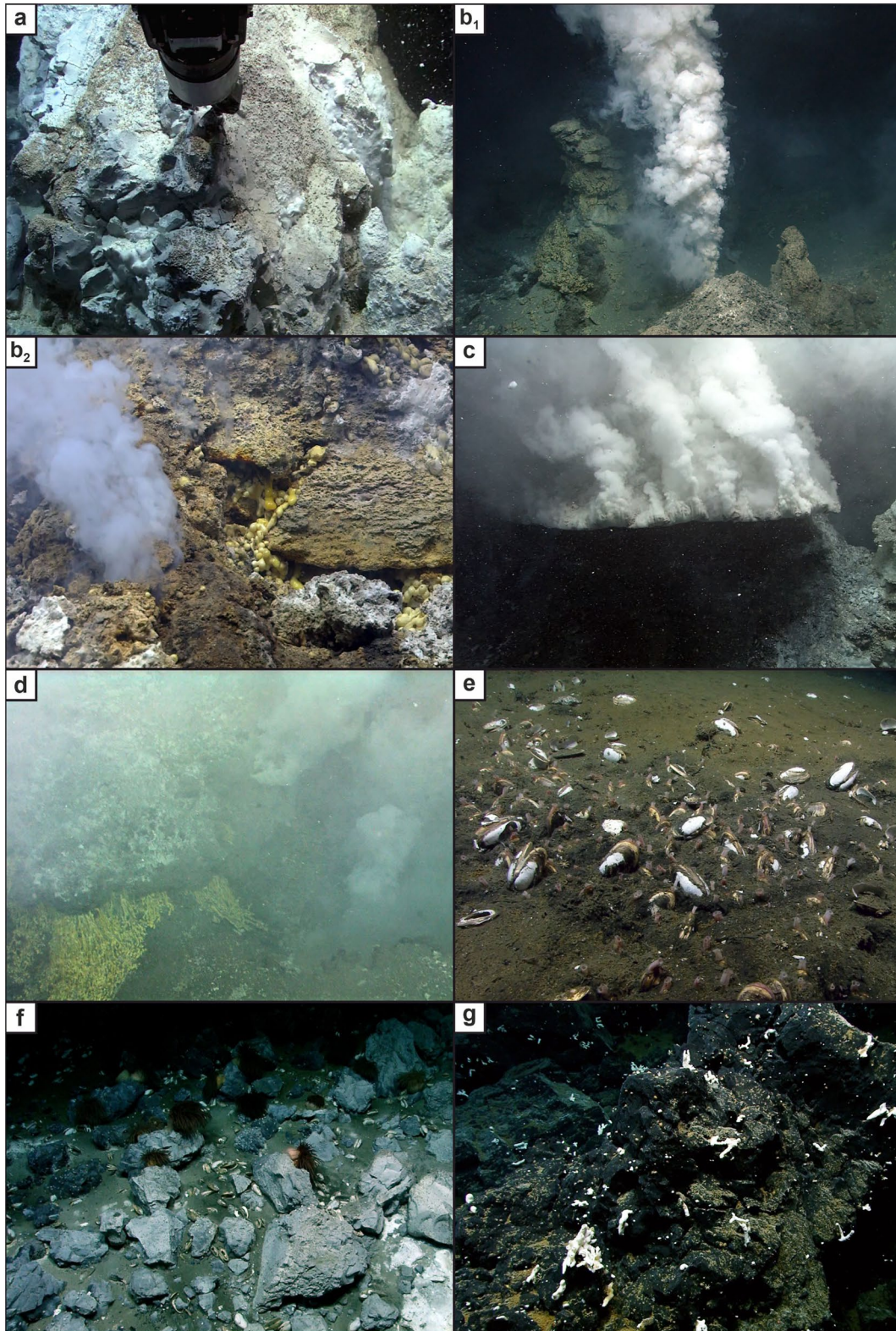


Figure 5.

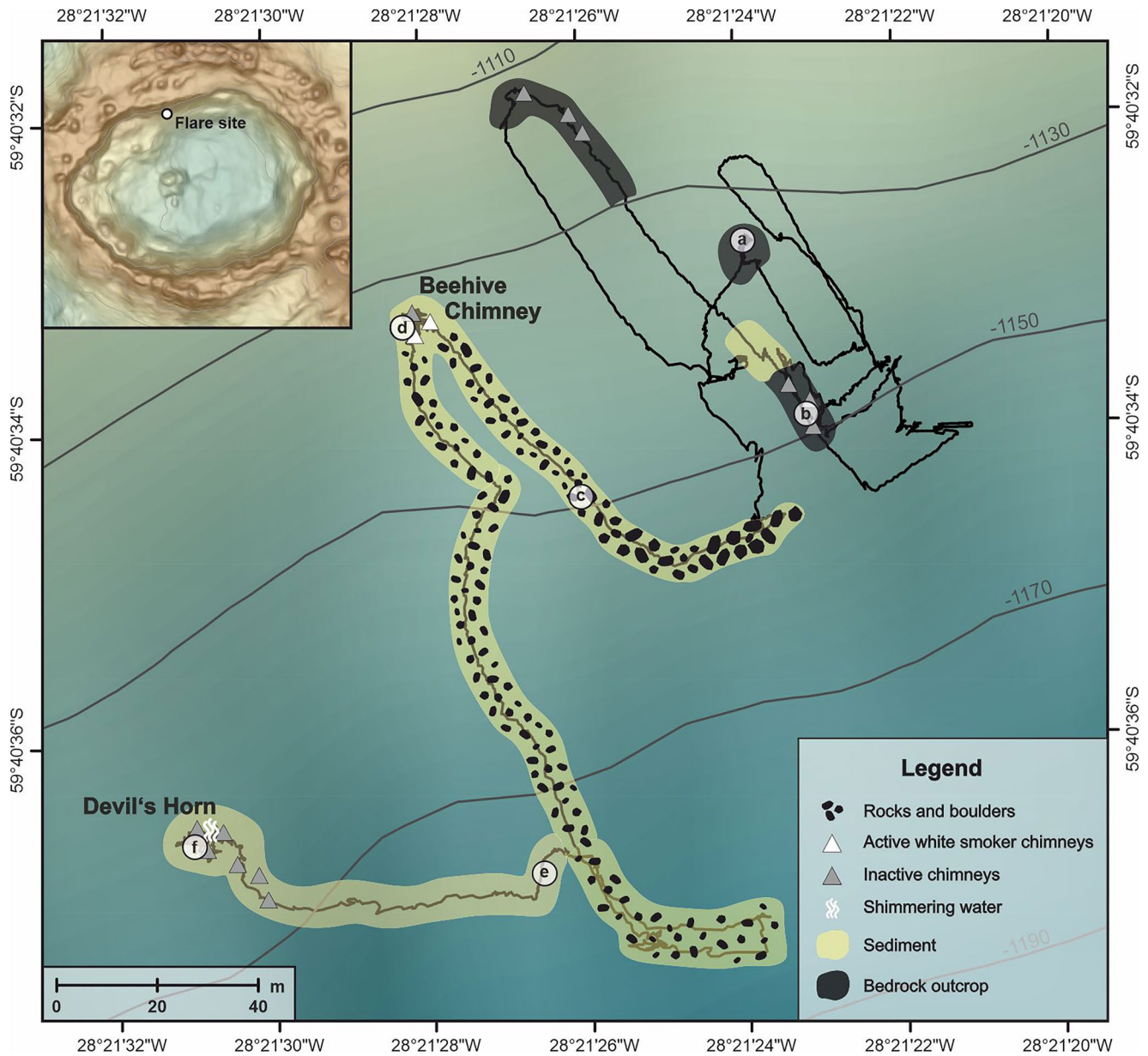


Figure 6. Map created from visual remotely operated vehicle (ROV) seafloor observations (ROV 449) of the flare site with the newly discovered Beehive Chimney site (59°40'33.24"S, 28°21'28.02"W). During the first half of the dive, bottom visibility was not always assured as the water column was searched for the source of the flare. The letters in this map refer to the corresponding letters of seafloor images in Figure 7.

4.3.1. Vent Field

The vent field is the most hydrothermally active area within the Kemp Caldera known so far, located in the caldera's center to the east of the resurgent cone. This area hosts several vent sites, including the Great Wall, Toxic Castle and Winter Palace. The vent field floor is mainly covered by sediment except for the slope side in the northwest, which is dominated by boulders and bedrock outcrops (Figures 4 and 5g). Downslope to the east,

Figure 5. Seafloor images showing (a) Rock sampling from a wall-like structure at the Great Wall. The wall consists of weathered rock, which is partly covered by fine-crystalline sulfur, microbial mats and limpets, (b₁) Actively venting white smoker at Toxic Castle, (b₂) Liquid sulfur at Toxic Castle dripping out of the rock and rapidly cools to sulfur spherules, (c) Flange structure (Toxic Castle), from which hot water rises from below and turn into white smoke, (d) Liquid elemental sulfur at Winter Palace, similar to that found at Toxic Castle. However, the visibility was much worse here because of the turbidity caused by the actively venting white smokers. (e) Clam shells and living clams on sediment field northwest of Toxic Castle. (f) Sediment covered with boulders of different sizes, which are slightly too strongly weathered, and (g) Bedrock partly overgrown with sponges.

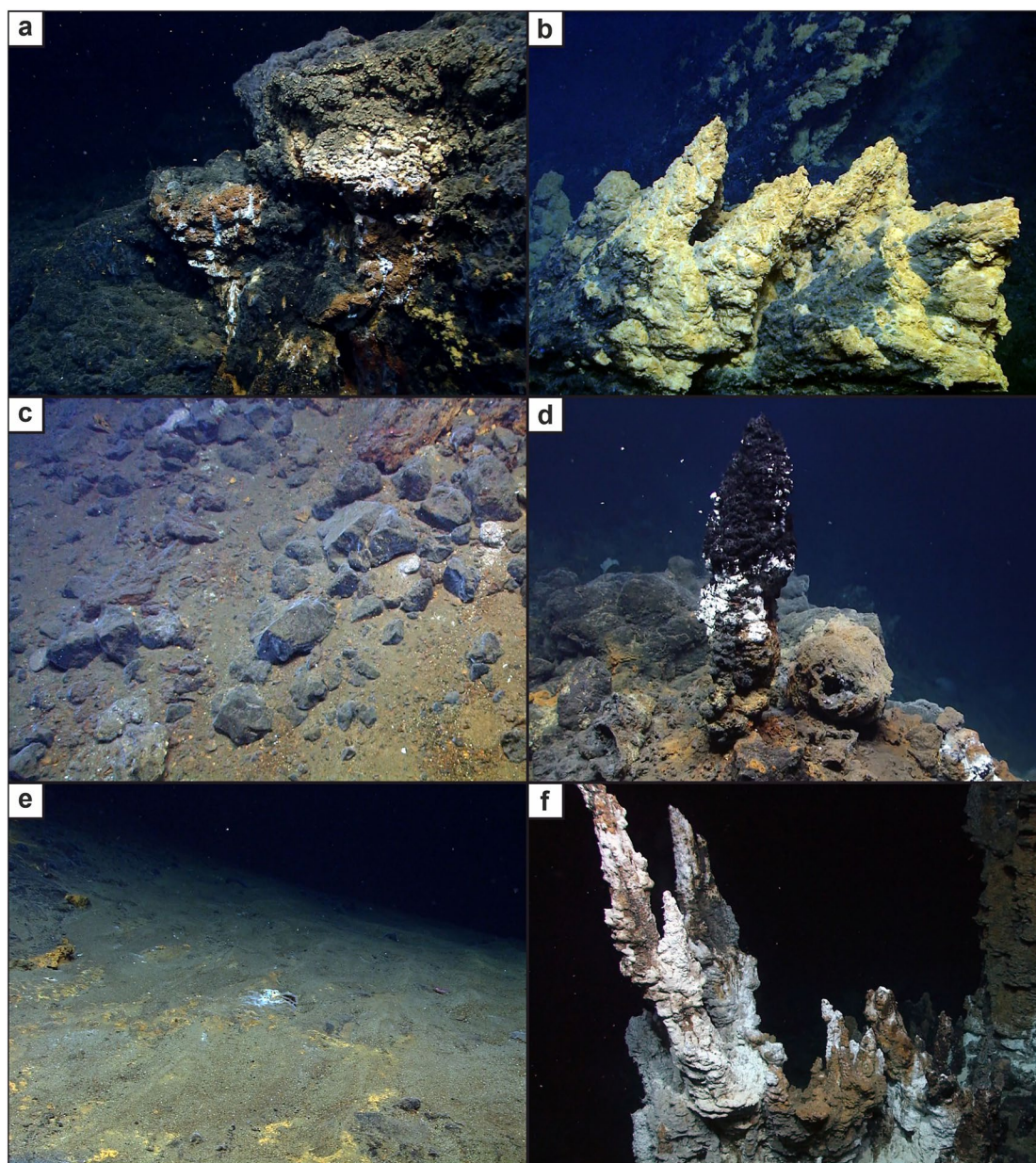


Figure 7. Underwater images from several areas within the flare site. (a) Bedrock outcrop partly weathered with brownish stains, (b) Partially weathered (yellowish material) chimney-like structures, (c) Sediment with boulders on top. The sediment shows a brownish discoloration in some places as well as in some of the rock pieces (upper right corner of the image), (d) Actively venting beehive-shaped chimney at the newly discovered Beehive Chimney site. Beside the big chimney, some smaller and also active chimneys were found next to old, inactive ones, (e) Wide sediment-covered area with only a few spots with discoloration and microbial mats, and (f) Oblique plan view of the biggest chimney structure at the location Devil's Horn.

the bedrock is increasingly covered by sediments, but boulders and smaller rocks are still visible on the top of the sediment. The white smoker vent sites Toxic Castle and Winter Palace, where small white smoker chimneys and mounds are present, are sediment-dominated.

The Great Wall, one of the hydrothermally active sites in this area, is located at a water depth of $\sim 1,416$ m at the eastern flank of the resurgent cone. The wall-like structure from which this site owes its name, mainly consists of weathered rock (Figure 5a). In some places, the wall is covered by microbial mats, limpets, and fine-crystalline elemental sulfur. In addition to the Great Wall, such sulfur walls also exist in the surrounding area, where sulfur-bearing hydrothermal fluids escape through fissures and cracks in the seafloor (Figure 4). The area around the Great Wall is mainly sediment-covered ground with some larger and smaller boulders on top (Figures 5a and 5f). Downslope toward both the Toxic Castle and Winter Palace vent fields, these boulders decrease in size.

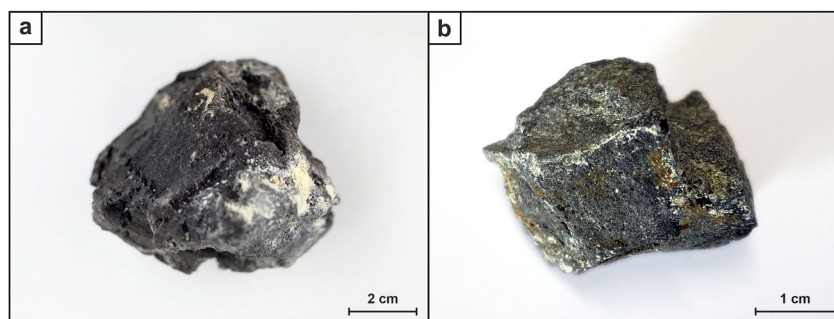


Figure 8. Rock samples from the Great Wall. (a) Sample 028-5R recovered from the foot of the wall structure, and (b) A smaller piece of the sample 028-6R, which was taken directly from the wall.

Toxic Castle is located <80 m east-southeast of the Great Wall and its morphological features are different compared to its western neighbor site. This actively venting area hosts several white smoker chimneys and mounds (Figure 5b₁). An interesting phenomenon of this site is the occurrence of liquid elemental sulfur (Figure 5b₂). At some spots, the liquid sulfur drips out of the rock and rapidly cools to sulfur spherules. At other places, the sulfur is already solidified to sulfur drops covering some of the mounds. We also discovered a flange structure at Toxic Castle, from which hot water rose from below and turned into white smoke (Figure 5c).

Winter Palace, like Toxic Castle, is an active white smoker vent field and is located at a water depth of ~1,422 m. Unfortunately, due to low visibility caused by the white smokers, fewer features could be distinguished than at the other locations. However, also here liquid elemental sulfur was discovered in patches (Figure 5d). To the north, about halfway from the Great Wall to the Toxic Castle, a clam field was present in a small depression (Figure 5e). This sediment patch, hosting living clams, lies between hillocks and is covered by sediment and small boulders.

The Kemp Caldera sediments are mainly composed of shards of local volcanic rocks, quartz, plagioclase feldspars, sulfides (especially sphalerite and pyrite) and plume fall-out particles from hydrothermal vents. Thus, elemental sulfur is found in the sediments at Toxic Castle, Winter Palace and Great Wall (cf., Hepburn, 2015). Biogenic opal ooze composed of Antarctic Polar Front diatoms was also found in the sediment, but only in the deepest part of the caldera.

4.3.2. Flare Site

The flare site is located at the NNW rim of the Kemp Caldera at a water depth between 1,110 and 1,190 m. Due to the detection of a gas flare at this site with the echosounder of the vessel (producing an acoustic anomaly), the ROV was deployed to further investigate the area on the seafloor. As displayed in the map (Figure 6), there was not always visual ground contact because the first half of the dive was used to find the rising gas bubbles in the water column with use of the ROV mounted forward looking sonar. Hence, visual seafloor mapping of the flare site was restricted to the second part of the dive.

ROV dive 449 started in the northeastern part of the flare site, trying to localize the source of the gas bubbles, which was unfortunately not detected. During short moments of ground visibility, bedrock outcrops (Figure 7a) and old, inactive chimney structures (Figure 7b) were visible. After finishing the search for the gas bubble source, the area was further investigated regarding possible hydrothermally active sites. At a water depth of ~1,135 m (about 400 m from the upper caldera edge) on a 32° sloping caldera floor, a new site was discovered, named Beehive Chimney. This actively venting beehive-shaped chimney is surrounded by boulders, and inactive chimneys were found in the immediate vicinity (Figure 7d). The area south of Beehive Chimney is predominantly sediment covered with boulders (Figure 7c). It can be assumed that these boulders have fallen from the caldera wall. Further south, the boulders decrease in size or are no longer present, leaving some areas covered only by sediment (Figure 7e). In the southwest of the flare site area, a second vent field was found, named Devil's Horn (Figure 6). This area hosts a large field of high chimney structures, but none of them were actively venting. At the base of a particularly impressive white-coated chimney structure, shimmering water was observed (fluid temperature of 198.3°C).

4.4. Mineralogy and Chemical Composition of Rock Samples

Three rock samples were taken from the vent site in the center of the Kemp Caldera. Polished thin sections were made of these samples and studied with transmitted light microscopy for mineral identification. Detailed micro-

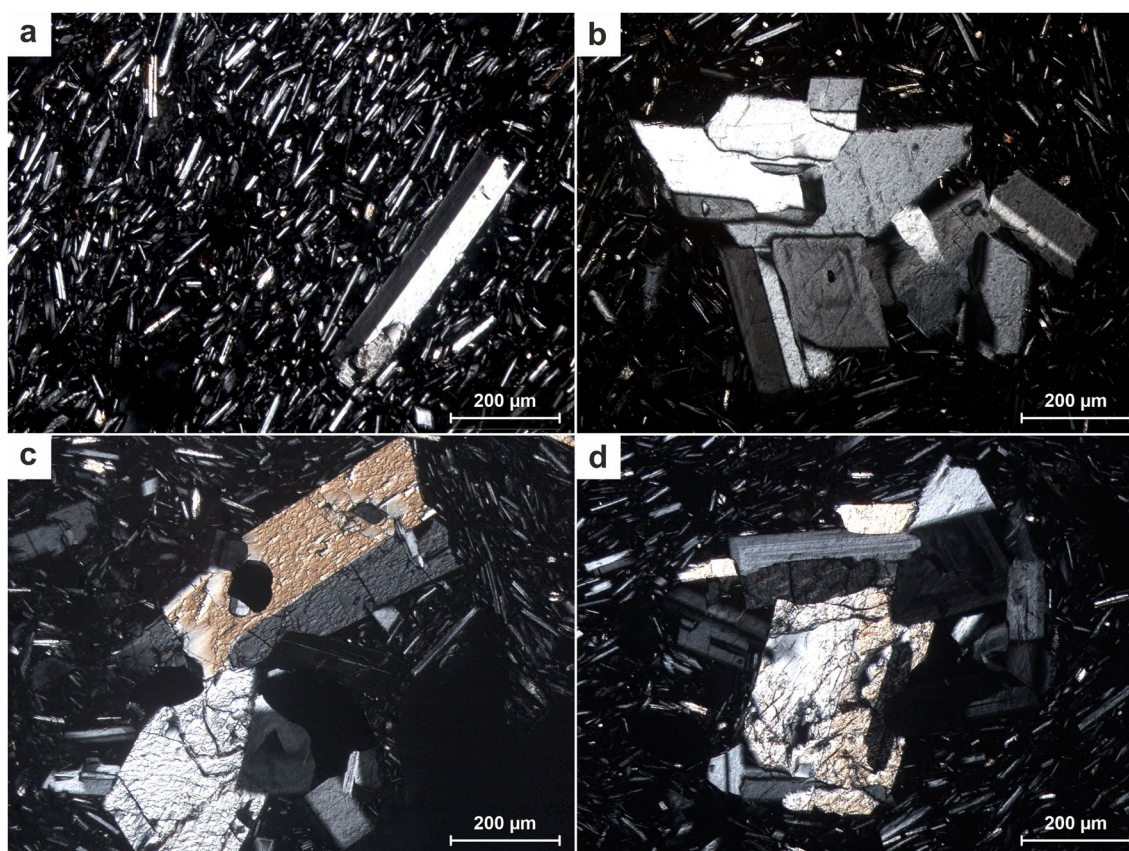


Figure 9. Detailed microscopic images (crossed polarized transmitted light) of thin sections made from Great Wall rock samples 028-5R and 028-6R. (a) Glassy matrix and acicular plagioclase crystals with a plagioclase phenocryst. A slight intimation of a flow texture can be seen, as most of the plagioclase crystals are oriented in one direction, (b) Accumulation of tabular to prismatic plagioclase crystals, (c) Twinned clinopyroxene phenocrysts within plagioclase-rich matrix, and (d) Mineral accumulation consisting of a ca. 500 μm sized twinned clinopyroxene crystal (resorption texture at right crystal edge) and several smaller plagioclases.

photographs of the thin sections are shown in Figure 9. Furthermore, XRF analysis was used to determine the chemical composition of the rock samples (Table 2).

Two of the three rock samples were taken from the Great Wall. One rock piece (028-5R) was taken from the foot of the wall structure, and the other one (028-6R) was sampled directly from the wall itself. The third sample was taken from a clam field (033-3B). This sample actually consists of several smaller rock pieces because a whole shovel of loose material was taken. All samples have a dark gray to black color and occasionally brownish stains. Fine-crystalline sulfur adheres to the rough surface of the rocks sampled at the Great Wall (Figure 8). In the handpiece, the surfaces are slightly shiny and vesicles in the size of <1 mm are visible.

The samples have a porphyritic texture. Their matrix is glassy and contains acicular plagioclase micro-phenocrysts (<150 μm) that are locally aligned (Figure 9). Plagioclase and clinopyroxene in the size of >200 μm occur as single phenocrysts or in mineral accumulations (small xenoliths).

Table 2
Chemical Composition Determined Through X-Ray Fluorescence Analysis of the Three Rock Samples Taken From the Vent Field Site in the Center of the Kemp Caldera

Sample ID	SiO ₂	TiO ₂	Al ₂ O ₃	Fe ₂ O ₃	MnO	MgO	CaO	Na ₂ O	K ₂ O	P ₂ O ₃	Sum
028-5R	67.68	0.64	13.50	6.53	0.16	1.06	4.35	4.16	1.01	0.22	99.31
028-6R	67.40	0.64	13.39	6.38	0.15	1.09	4.35	4.19	1.02	0.23	98.84
033-3B	67.72	0.65	13.46	6.67	0.15	1.06	4.35	4.24	1.00	0.23	99.53

Note. All values are given in weight% (wt%).

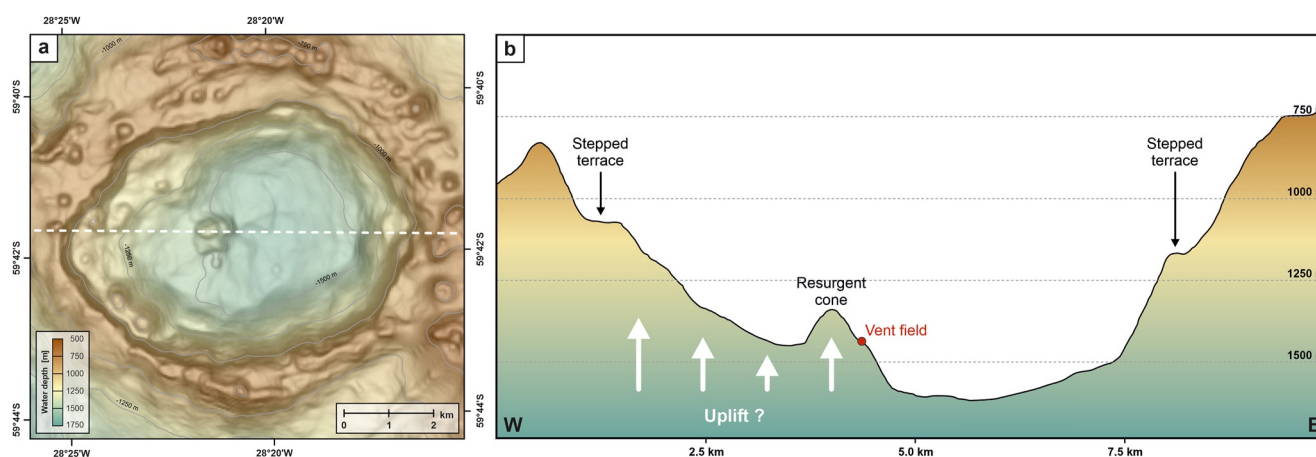


Figure 10. (a) Bathymetric map of the Kemp Caldera showing the position of the profile (dashed white line) trending from W to E, and (b) W–E bathymetric profile through the Kemp Caldera.

XRF analysis of the rocks sampled at the vent field of the Kemp Caldera revealed an SiO_2 content of more than 67 wt% and alkali contents of ca. 5.2 wt% (Table 2), indicating a dacitic composition of the rocks according to the total alkali silica classification (TAS; LeBas et al., 1986). Considering the high content of Fe_2O_3 , relatively low MgO content and about 1% K_2O (Table 2), the Kemp Caldera samples from the resurgent cone fall in the tholeiitic field of the AFM diagram (cf., Vermeesch & Pease, 2021) rather than the low-K tholeiitic series to which the volcanic rocks of the South Sandwich island arc belong (e.g., Leat et al., 2003).

5. Discussion

5.1. Geomorphology of the Kemp Caldera and Distribution of Hydrothermal Vents

The morphology of the Kemp Caldera resembles that of a resurgent caldera (J. W. Cole et al., 2005). In the central part of a caldera, resurgence often occurs due to refilling of the subvolcanic magma reservoir, which causes uplift of the caldera floor (Acocella, 2021; Lipman, 1997; Smith & Bailey, 1968). However, the process of resurgence of a caldera usually results in uplift and doming of the entire caldera floor, which is not the case for the Kemp Caldera. The asymmetry of the caldera floor in the Kemp Caldera could be caused by uplift, which affects only the western part of the caldera (Figure 10). The morphology of the central cone suggests that it is an extrusive (resurgent) cone as a result of at least one post-caldera eruption, while the uplift of the western caldera floor may be caused by a spatially restricted shallow intrusion.

The fact that the caldera floor in the western part is generally shallower than the eastern caldera floor could depend on the interaction of different factors. Post-caldera eruption(s), which built the resurgent cone in the center of the caldera, may have been accompanied by differential uplift caused by refilling of an underlying magma chamber. This small intrusion may have led to an inhomogeneous uplift of the caldera floor that affected only the western part of the caldera and left the eastern caldera floor nearly unchanged. The collapse of unstable caldera walls may also have modified the morphology of the caldera floor and the caldera itself. Collapse of steep walls formed during the first caldera forming event(s) and rapid subsidence of the inner caldera floor may have resulted in gravitational mass wasting and localized deposition of debris flow deposits on the caldera floor. Uplift-induced movement during the post-caldera magma movements and eruption(s) might have triggered further caldera wall collapse and debris flow deposition.

Stepped terraces are seen as distinct edges at a water depth of $\sim 1,070$ m to the west and $\sim 1,170$ m to the east (Figure 10b). These terraces may represent collapse scars that modified the caldera wall. Alternatively, an older caldera wall or a former caldera floor from a previous collapse. Some calderas are formed not only from a single caldera-forming event but also undergo several effusive or explosive eruptions that cause repeated

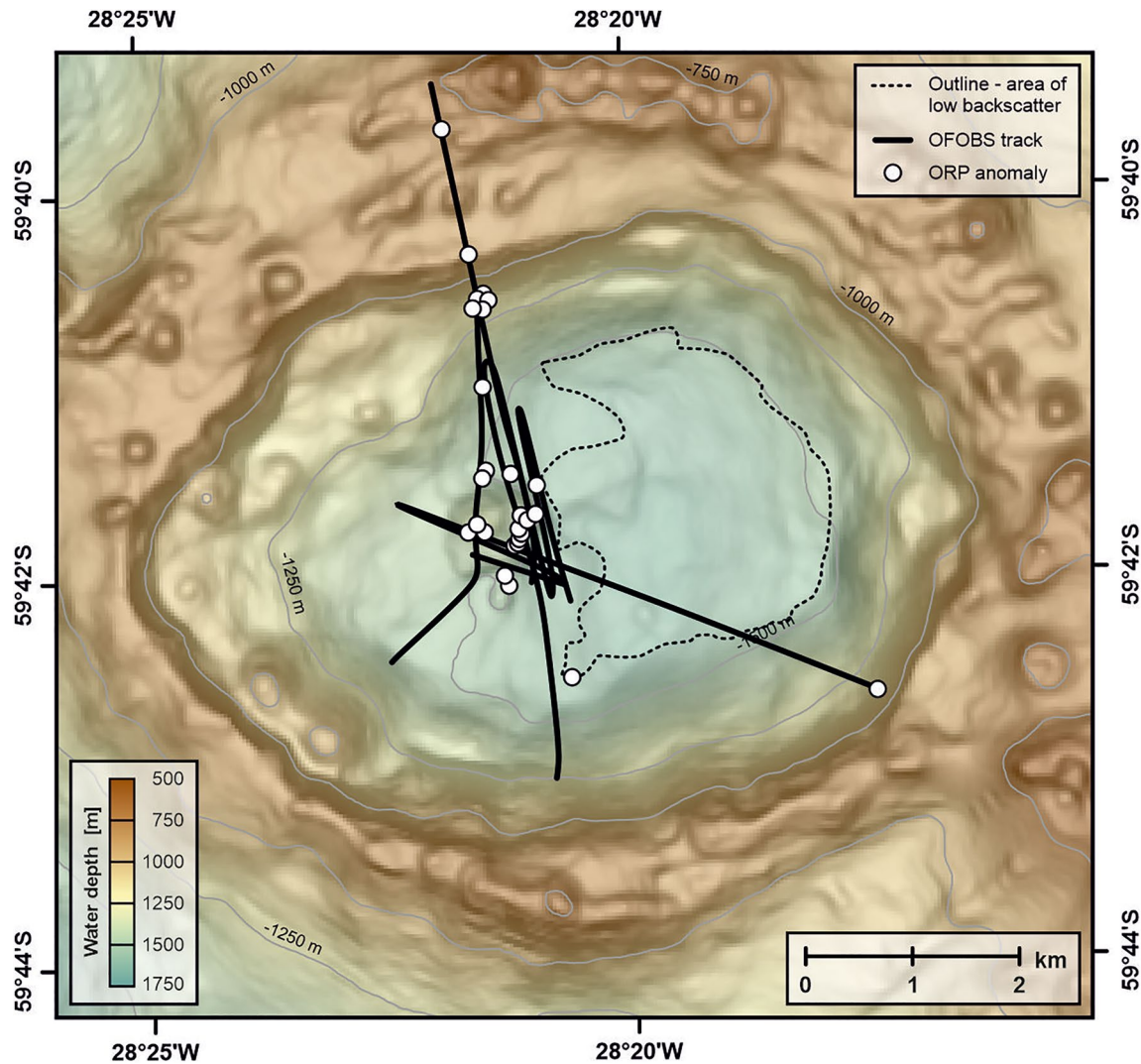


Figure 11. The distribution of oxidation-reduction potential (ORP) anomalies with dE/dt values < -0.02 mV/S are plotted in the map (ORP anomaly data on pers. comm. with T. Pape).

subsidence events (Branney & Acocella, 2015). Based on the observed morphology, it is suggested that the Kemp Caldera was formed due to at least two caldera collapse phases associated with magma withdrawal. Therefore, a shallow magma chamber below the current caldera must have existed. The collapse of a volcanic edifice due to withdrawal of magmatic supply has formed the first caldera, resulting in ring faults and other fractures caused by subsidence (Acocella et al., 2012; Branney, 1995). Thus, the outer caldera rim represents the first and thus older caldera, while the inner terraces mark a younger caldera formed by a second collapse event. However, deep-reaching ring faults could not be identified by the ship's hull-mounted hydroacoustic tools and its limited resolution. Despite that, the caldera walls are expressions of ring faults at the seafloor and the distribution of the small secondary cones along the caldera rim may indicate the position of ring faults if they have acted as magma conduits.

In most cases, these ring faults and fractures occur close to the caldera margin as this is the area of main faulting and intense deformation (Branney & Acocella, 2015). These faults connect the subvolcanic magma reservoir with the seafloor and can act as pathways for infiltrating seawater and related hydrothermal fluids (e.g., Acocella, 2021; Berkenbosch et al., 2015; de Ronde et al., 2011; Klose et al., 2022). Consequently, hydrothermal

Table 3
Diverse Features of Kemp Caldera Compared to the Two Submarine Caldera Volcanoes, Brothers and Niutahi

Features	Brothers volcano ^a	Niutahi volcano ^b	Kemp Caldera
Location	South of Kermadec arc (SW Pacific)	NE Lau Basin (SW Pacific)	South Sandwich island arc (South Atlantic)
Caldera diameter	3.0 × 3.4 km	~10 km	6.5 × 8.6 km
Caldera depth	~1,879 m	~1,700 m	~1,618 m
Rock composition	Predominantly dacitic	Dacitic (low- and high-K)	Dacitic
Post-caldera cones	2 cones: Lower Cone and Upper Cone	4 cones: Central, SE, SW and Northern Cone	1 cone: resurgent cone in western center
Location of active hydrothermal vents	NW Caldera, Lower Cone, Upper Cone	South of Central Cone, SW Cone, Northern Cone	Central vent field, flare site at NNW caldera rim

^aTaken from de Ronde et al. (2005) and Berkenbosch et al. (2015). ^bTaken from Kim et al. (2011) and Peters et al. (2021).

activity and intense hydrothermal alteration in (submarine) calderas predominantly occur at the caldera rims (Berkenbosch et al., 2015; Branney & Acocella, 2015; Eddy et al., 1998). At Kemp Caldera, such a hydrothermally active site probably related to faults close to the caldera rim has been identified, the Beehive Chimney at the flare site at the NNW caldera rim. However, the hydrothermal activity in the Kemp Caldera is not only found at its rim but also within the vent field around the resurgent cone. In calderas where resurgence occurs, the uplifted area is typically intersected by minor faults and fissures (Acocella, 2021; Branney & Acocella, 2015). In the case of the Kemp Caldera, this concerns the central area around the resurgent cone. Extrusive volcanism and the supply of fresh lava may have formed small faults around the cone, where hydrothermal flow and heat flow have been focused.

A (temporal) change in hydrothermal activity is especially seen in the vent field hydrothermal fluids and their change in temperature. Fluids of the Great Wall sampled and measured during the R/V *James Cook* cruise JC42 reached temperatures of 21.1°C (C. S. Cole et al., 2014; Rogers, 2010), while the fluids of the same site measured in 2019 during the R/V *Polarstern* cruise PS119 have temperatures of 63°C (Kürzinger et al., 2022). Simultaneously, a temperature increase is observed in the Toxic Castle fluids. This area was previously known as the diffuse fluid flow area (Hepburn, 2015; Tyler, 2011), which generally indicates relatively low temperatures; however, in 2019, measured fluid temperatures ranged from 207 to 237°C (Kürzinger et al., 2022). This temperature increase could be evidence of recent magma activity and magma movement to shallower levels.

Hydrothermal activity present in the western part of the caldera in contrast to its eastern part is also seen in the results shown by mapping the oxidation-reduction potential (ORP) anomalies (T. Pape, pers. comm.). ORP anomalies are exclusively detected in the western part (Figure 11). Such anomalies were measured using ORP sensors that respond to the presence of reduced hydrothermal chemicals, for example, HS⁻, H₂ and Fe²⁺ (Walker et al., 2007). Hence, ORP anomalies are related to hydrothermal activity, which in case of the Kemp Caldera mainly occurs around the resurgent cone and close to the caldera rim (T. Pape, pers. comm.).

5.2. Formation and Evolution of the Kemp Caldera

Every rock (sample) has a “geological fingerprint,” which means that the texture, structure and composition of the rock can be used to make statements about its formation and origin. In the case of the Kemp Caldera, it was previously assumed that the rock type of the caldera is the same as that of the neighboring Kemp Seamount, which consists primarily of tholeiitic basalt and basaltic andesite with SiO₂ contents between 50 and 53 wt% (C. S. Cole et al., 2014; Leat et al., 2004, 2013). The samples from the Kemp Caldera vent field, however, have much higher SiO₂ content. With SiO₂ >67 wt%, the sampled rocks clearly exceed the SiO₂ content of basalt or basaltic andesite and point to more silicic/felsic volcanic rocks. This matches our seafloor observations of relatively fresh blocky lava around the cone structure (see Figure 3c), a feature typical for dacitic volcanism.

Even if the composition of the rocks from the caldera center is different from that of Kemp Seamount, there are unfortunately no rock samples from the outer rim of the caldera. The only information about Kemp Caldera rocks from the NW caldera wall is provided in the JR224 cruise report (Larter, 2009), which states, on the basis of visual observation, that the caldera walls consist of hexagonal basalt pillars. However, neither samples nor rock data exist. Considering that glassy dacite samples can also be dark in appearance and can also form hexagonal pillars, it cannot be ruled out that the rocks outside the center are dacitic and hence different from those of Kemp Seamount.

It can be assumed that both Kemp Seamount and the former “Kemp Volcano” (which later collapsed to form Kemp Caldera) were formed by basaltic to rhyolitic volcanism resulting from the ongoing subduction of the South American Plate under the Sandwich micro-plate (Barry et al., 2006; Larter et al., 1998; Leat et al., 2004). It is possible that the erupted material forming these two seafloor features had a rock composition of tholeiitic basalt to basaltic andesite (C. S. Cole et al., 2014; Leat et al., 2004, 2013). Later, magma withdrawal of the subvolcanic magma chamber caused the collapse of the “Kemp Volcano” and led to the formation of the Kemp Caldera. Resurgence and uplift are commonly initiated relatively soon

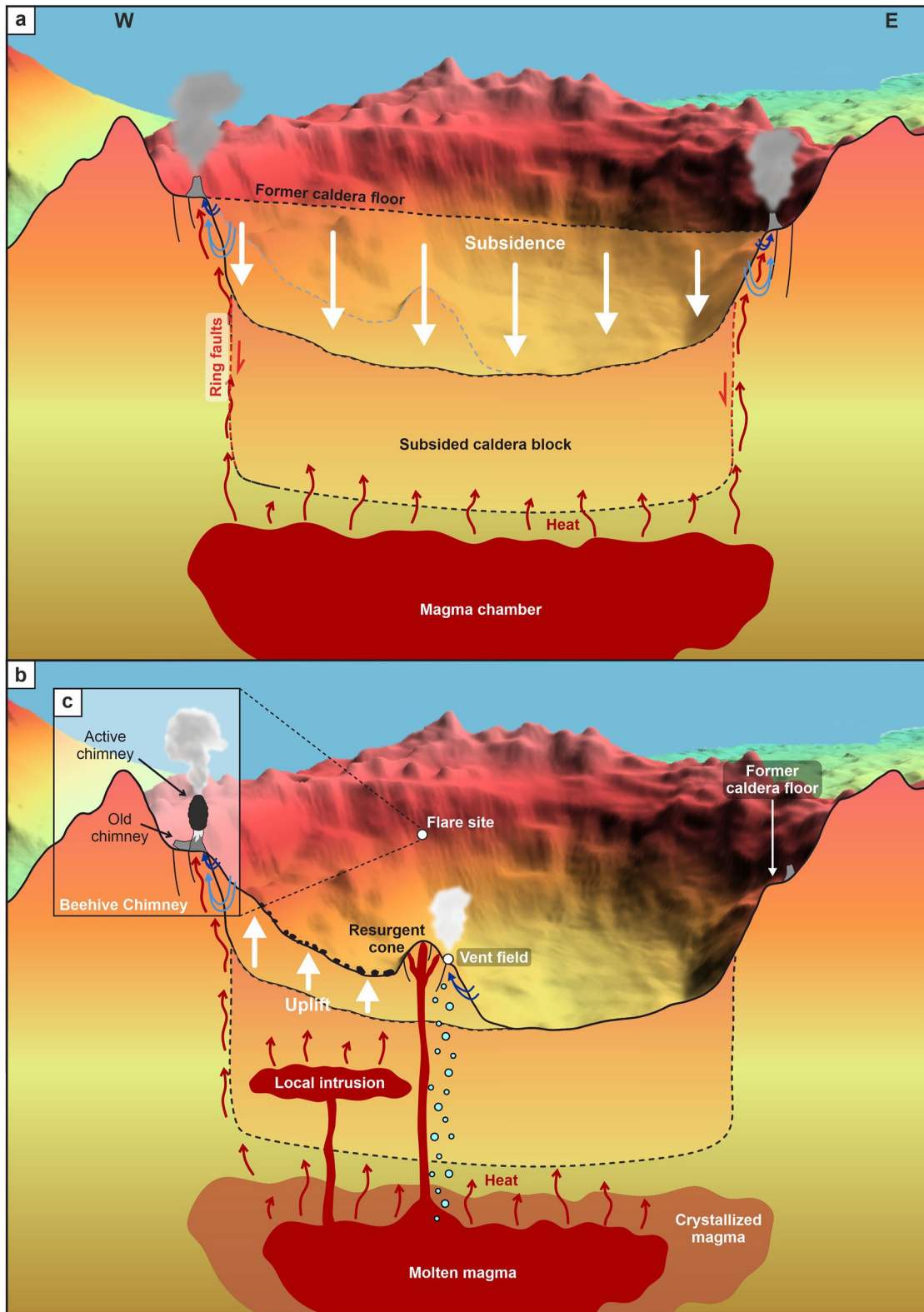


Figure 12.

after the caldera collapse event(s), in the range of 10 a to 100 ka (Branney & Acocella, 2015; Nielson & Hulen, 1984). This uplift takes place when new magma refills the shallow reservoir. The now erupted material had a more felsic (dacitic) composition, which indicates that the magma that resided in the partially drained subvolcanic magma reservoir remained there long enough to become more siliceous than the initially erupted magma (cf., J. W. Cole et al., 2005). Thus, this might lead to the two different rock types that are found within the Kemp Caldera.

Another possibility is that the entire Kemp Caldera is of dacitic composition. The composition of magmas that are associated with subduction-related volcanism varies with increasing distance to the subduction front (Duggen et al., 2007). Rear-arc magmas are generally more siliceous than the magmas of the volcanic arc itself (Duggen et al., 2007). Two examples of submarine caldera volcanoes of broadly similar rock composition are Brothers volcano (Kermadec arc) and Niuatahi volcano (NE Lau Basin), which are similar in shape and size to Kemp Caldera (Table 3). Brothers and Niuatahi are predominantly dacitic in composition and also have dacite post-caldera cones within the caldera (Berkenbosch et al., 2015; de Ronde et al., 2011, 2019). Due to the rear-arc position of the Kemp Caldera, it appears possible that the Kemp Caldera was also formed by dacitic volcanism. Further rock sampling at Kemp Caldera and especially at its rim is needed to resolve its composition and finally its evolution.

6. Conclusions

The results of this study provide detailed visual seafloor observations and descriptions of the bathymetric characteristics of the Kemp Caldera and the hydrothermal vent areas detected at the caldera rim and floor. We assume that the caldera was formed by at least two collapse events: the stepped terraces inside the caldera indicate a younger caldera, while the outer rim represents an even older caldera structure (Figure 12). The asymmetry of the caldera floor may result from uplift caused by a local intrusion. Additional mass wasting events may have occurred due to the instability of the caldera walls, enhancing the asymmetry of the floor.

The focus of hydrothermal activity, which is also confirmed by anomalies of mapped ORP, is the dacitic resurgent cone in the central area of the Kemp Caldera and the NNW caldera rim. This cone may be the result of one or more post-caldera eruptions of differentiated magma, leading to the extrusion of blocky, dacitic lava. Heat flow is focused at the resurgent cone, resulting in a temperature increase in hydrothermal fluids of the vent field that may be the result of a recent movement of magma to a shallower level as a subvolcanic intrusion.

The former suggestion that Kemp Caldera may be composed of the same rock type as Kemp Seamount was based only on the fact that hexagonal columns, interpreted as basalt columns, have been seen on the NW caldera rim during the JR224 R/V *James Clark Ross* cruise in 2009 (Larter, 2009). However, to verify the rock composition of the entire caldera, it would be necessary to investigate further rock samples.

Figure 12. Schematic drawing of the Kemp Caldera (cross-section from W to E) to illustrate its formation and development. (a) Sketch of a subsidence event as a result of magma chamber roof collapse due to magma withdrawal after the first caldera-forming collapse event, represented by the outer caldera rim. The resulting ring faults close to the caldera rim may have acted as magma conduits, leading to the formation of the small secondary cones, and pathways for infiltrating seawater (dark blue-colored arrows) and hydrothermal fluids (light blue-colored arrows), which is seen, for example, at the flare site, (b) Present state of the Kemp Caldera. A local intrusion may have caused the uplift of the western caldera floor. One or more post-caldera eruptions in the central part have caused the development of the resurgent cone, which also led to the formation of fissures and small faults. Due to these new pathways for hydrothermal fluids, heat flow as well as hydrothermal flow could focus on the cone in addition to the hydrothermal activity close to the caldera rim. The vent field, located at the eastern flank of the resurgent cone, is dominated by white smoker vents, accompanied by the formation of fine-crystalline and liquid elemental sulfur, and (c) Beehive Chimney at the flare site at the NNW caldera rim. At this site, inactive chimneys were found beside actively venting chimneys.

Data Availability Statement

Multibeam echosounder bathymetry and ORP anomalies are reported in the cruise report of the expedition PS119 of the Research Vessel POLARSTERN to the Eastern Scotia Sea in 2019 (Bohrmann, 2019a). Raw data and products of hydroacoustic data collected during PS119 are available via the World Data Center PANGAEA Data Publisher for Earth & Environmental Science: Bohrmann (2019b) and Wintersteller et al. (2023).

Acknowledgments

Many thanks go to Captain M. Langhinrichs and the crew from the R/V *Polarstern* PS119 cruise. Their support and cooperation with the ROV *MARUM QUEST 4000* team was excellent. Special thanks go to P. Wintersteller, who was responsible for the acquisition of bathymetric data and supported the OFOBS dives during the PS119 expedition. Thanks also go to A. Klügel (University of Bremen, Germany), who supported the work with his knowledge about volcanoes and calderas. AL thanks the Hanse-Wissenschaftskolleg Institute for Advanced Study for their support during the final preparation stages of this manuscript. The PS119 expedition was funded by the BMBF via Projektträger (03G0880A) and the DFG within the Cluster of Excellence (EXC-2077, project number 390741603 “The Ocean Floor—Earth’s Uncharted Interface”) at MARUM—Center for Marine and Environmental Sciences, University of Bremen. Open Access funding enabled and organized by Projekt DEAL.

References

- Acocella, V. (2021). Calderas. In *Volcano-tectonic processes* (pp. 163–203). Springer. https://doi.org/10.1007/978-3-030-65968-4_5
- Acocella, V., Palladino, D. M., Cioni, R., Russo, P., & Simei, S. (2012). Caldera structure, amount of collapse, and erupted volumes: The case of Bolsena caldera, Italy. *GSA Bulletin*, 124(9/10), 1562–1576. <https://doi.org/10.1130/b30662.1>
- Amon, D. J., Glover, A. G., Wiklund, H., Marsh, L., Linse, K., Rogers, A. D., & Copley, J. T. (2013). The discovery of a natural whale fall in the Antarctic deep sea. *Deep Sea Research Part II: Topical Studies in Oceanography*, 92, 87–96. <https://doi.org/10.1016/j.dsr2.2013.01.028>
- Arango, C. P., & Linse, K. (2015). New Sericosura (Pycnogonida:Ammonotheidae) from deep-sea hydrothermal vents in the Southern Ocean. *Zootaxa*, 3995(1), 37–50. <https://doi.org/10.11646/zootaxa.3995.1.5>
- Barry, T. L., Pearce, J. A., Leat, P. T., Millar, I. L., & Le Roex, A. P. (2006). Hf isotope evidence for selective mobility of high-field-strength elements in a subduction setting: South Sandwich Islands. *Earth and Planetary Science Letters*, 252(3–4), 223–244. <https://doi.org/10.1016/j.epsl.2006.09.034>
- Berkenbosch, H. A., de Ronde, C. E. J., Gemmill, J. B., McNeill, A. W., & Goemann, K. (2012). Mineralogy and Formation of black smoker chimneys from Brothers submarine volcano, Kermadec arc. *Economic Geology*, 107(8), 1613–1633. <https://doi.org/10.2113/econgeo.107.8.1613>
- Berkenbosch, H. A., de Ronde, C. E. J., Paul, B. T., & Gemmill, J. B. (2015). Characteristics of Cu isotopes from chalcopyrite-rich black smoker chimneys at Brothers volcano, Kermadec arc, and Niutaahi volcano, Lau basin. *Mineralium Deposita*, 50(7), 811–824. <https://doi.org/10.1007/s00126-014-0571-y>
- Bohrmann, G. (2019a). *The Expedition PS119 of the Research Vessel POLARSTERN to the Eastern Scotia Sea in 2019, Reports on Polar and Marine Research*. Alfred-Wegener-Institut, Helmholtz-Zentrum für Polar- und Meeresforschung. https://doi.org/10.2312/BZPM_0736_2019
- Bohrmann, G. (2019b). Links to master tracks in different resolutions of POLARSTERN cruise PS119, Punta Arenas - Port Stanley, 2019-04-13 - 2019-05-31 [Dataset]. Alfred Wegener Institute, Helmholtz Centre for Polar and Marine Research. <https://doi.org/10.1594/PANGAEA.904050>
- Branney, M., & Acocella, V. (2015). Calderas. In H. Sigurdsson & B. F. Houghton (Eds.), *Encyclopedia of volcanoes* (2nd ed., pp. 299–315). Elsevier/AP, Academic Press is an imprint of Elsevier. <https://doi.org/10.1016/B978-0-12-385938-9.00016-X>
- Branney, M. J. (1995). Downsag and extension at calderas: New perspectives on collapse geometries from ice-melt, mining, and volcanic subsidence. *Bulletin of Volcanology*, 57(5), 303–318. <https://doi.org/10.1007/bf00301290>
- Caress, D. W., Chayes, D. N., & dos Santos Ferreira, C. (2017). *MB-system: Mapping the seafloor*. Monterey Bay Aquarium Research Institute.
- Cole, C. S., James, R. H., Connelly, D. P., & Hathorne, E. C. (2014). Rare earth elements as indicators of hydrothermal processes within the East Scotia subduction zone system. *Geochimica et Cosmochimica Acta*, 140, 20–38. <https://doi.org/10.1016/j.gca.2014.05.018>
- Cole, J. W., Milner, D. M., & Spinks, K. D. (2005). Calderas and caldera structures: A review. *Earth-Science Reviews*, 69(1–2), 1–26. <https://doi.org/10.1016/j.earscirev.2004.06.004>
- de Ronde, C. E. J., Baker, E. T., Massoth, G. J., Lupton, J. E., Wright, I. C., Feely, R. A., & Greene, R. R. (2001). Intra-oceanic subduction-related hydrothermal venting, Kermadec volcanic arc, New Zealand. *Earth and Planetary Science Letters*, 193(3–4), 359–369. [https://doi.org/10.1016/S0012-821X\(01\)00534-9](https://doi.org/10.1016/S0012-821X(01)00534-9)
- de Ronde, C. E. J., Faure, K., Bray, C. J., Chappell, D. A., & Wright, I. C. (2003). Hydrothermal fluids associated with seafloor mineralization at two southern Kermadec arc volcanoes, offshore New Zealand. *Mineralium Deposita*, 38(2), 217–233. <https://doi.org/10.1007/s00126-002-0305-4>
- de Ronde, C. E. J., Hannington, M. D., Stoffers, P., Wright, I. C., Ditchburn, R. G., Reyes, A. G., et al. (2005). Evolution of a submarine magmatic-hydrothermal system: Brothers volcano, southern Kermadec arc, New Zealand. *Economic Geology*, 100(6), 1097–1133. <https://doi.org/10.2113/gsecongeo.100.6.1097>
- de Ronde, C. E. J., Humphris, S. E., Höfig, T. W., & Reyes, A. G. (2019). Critical role of caldera collapse in the formation of seafloor mineralization: The case of Brothers volcano. *Geology*, 47(8), 762–766. <https://doi.org/10.1130/G46047.1>
- de Ronde, C. E. J., Massoth, G. J., Butterfield, D. A., Christenson, B. W., Ishibashi, J., Ditchburn, R. G., et al. (2011). Submarine hydrothermal activity and gold-rich mineralization at Brothers Volcano, Kermadec Arc, New Zealand. *Mineralium Deposita*, 46(5–6), 541–584. <https://doi.org/10.1007/s00126-011-0345-8>
- de Ronde, C. E. J., & Stucker, V. K. (2015). Seafloor hydrothermal venting at volcanic arcs and backarcs. In H. Sigurdsson & B. F. Houghton (Eds.), *Encyclopedia of volcanoes* (2nd ed., pp. 823–849). Elsevier/AP, Academic Press is an imprint of Elsevier. <https://doi.org/10.1016/B978-0-12-385938-9.00047-X>
- Duggen, S., Portnyagin, M., Baker, J., Ulfbeck, D., Hoernle, K., Garbe-Schönberg, D., & Grassineau, N. (2007). Drastic shift in lava geochemistry in the volcanic-front to rear-arc region of the Southern Kamchatkan subduction zone: Evidence for the transition from slab surface dehydration to sediment melting. *Geochimica et Cosmochimica Acta*, 71(2), 452–480. <https://doi.org/10.1016/j.gca.2006.09.018>
- Eddy, C. A., Dilek, Y., Hurst, S., & Moores, E. M. (1998). Seamount formation and associated caldera complex and hydrothermal mineralization in ancient oceanic crust, Troodos ophiolite (Cyprus). *Tectonophysics*, 292(3–4), 189–210. [https://doi.org/10.1016/S0040-1951\(98\)00064-X](https://doi.org/10.1016/S0040-1951(98)00064-X)
- Fretzdorff, S., Livermore, R. A., Devey, C. W., Leat, P. T., & Stoffers, P. (2002). Petrogenesis of the back-arc East Scotia Ridge, South Atlantic Ocean. *Journal of Petrology*, 43(8), 1435–1467. <https://doi.org/10.1093/ptrology/43.8.1435>
- Georgieva, M. N., Wiklund, H., Bell, J. B., Eilertsen, M. H., Mills, R. A., Little, C. T. S., & Glover, A. G. (2015). A chemosynthetic weed: The tubeworm *Sclerolinum contortum* is a bipolar, cosmopolitan species. *BMC Evolutionary Biology*, 15(1), 280. <https://doi.org/10.1186/s12862-015-0559-y>
- German, C. R., Livermore, R. A., Baker, E. T., Bruguier, N. I., Connelly, D. P., Cunningham, A., et al. (2000). Hydrothermal plumes above the East Scotia Ridge: An isolated high-latitude back-arc spreading centre. *Earth and Planetary Science Letters*, 184(1), 241–250. [https://doi.org/10.1016/S0012-821X\(00\)00319-8](https://doi.org/10.1016/S0012-821X(00)00319-8)
- Hepburn, L. E. (2015). Hydrothermal sediment geochemistry south of the Antarctic Polar Front (Doctoral Thesis) (p. 484).
- Holdgate, M. W., & Baker, P. E. (1979). *The South Sandwich Islands: I. General description*. British Antarctic Survey.

- James, R. H., Green, D. R. H., Stock, M. J., Alker, B. J., Banerjee, N. R., Cole, C., et al. (2014). Composition of hydrothermal fluids and mineralogy of associated chimney material on the East Scotia Ridge back-arc spreading centre. *Geochimica et Cosmochimica Acta*, 139, 47–71. <https://doi.org/10.1016/j.gca.2014.04.024>
- Kim, J., Lee, K.-Y., & Kim, J.-H. (2011). Metal-bearing molten sulfur collected from a submarine volcano: Implications for vapor transport of metals in seafloor hydrothermal systems. *Geological Society of America*, 39(4), 351–354. <https://doi.org/10.1130/G31665.1>
- Kleint, C., Bach, W., Diehl, A., Fröhberg, N., Garbe-Schönberg, D., Hartmann, J. F., et al. (2019). Geochemical characterization of highly diverse hydrothermal fluids from volcanic vent systems of the Kermadec intraoceanic arc. *Chemical Geology*, 528, 119289. <https://doi.org/10.1016/j.chemgeo.2019.119289>
- Klose, L., Kleint, C., Bach, W., Diehl, A., Wilckens, F., Peters, C., et al. (2022). Hydrothermal activity and associated subsurface processes at Niutahi rear-arc volcano, North East Lau Basin, SW Pacific: Implications from trace elements and stable isotope systematics in vent fluids. *Geochimica et Cosmochimica Acta*, 332, 103–123. <https://doi.org/10.1016/j.gca.2022.06.023>
- Kürzinger, V., Diehl, A., Pereira, S. I., Strauss, H., Bohrmann, G., & Bach, W. (2022). Sulfur formation associated with coexisting sulfide minerals in the Kemp Caldera hydrothermal system, Scotia Sea. *Chemical Geology*, 606, 1–20. <https://doi.org/10.1016/j.chemgeo.2022.120927>
- Larter, R. D. (2009). The expedition JR224 of the RRS James Clark Ross in 2009. Chemosynthetically-driven Ecosystems South of the Polar Front consortium programme, *Multidisciplinary exploration to constrain hydrothermal vent and cold seep locations in the Scotia Sea*. Retrieved from https://www.bodc.ac.uk/resources/inventories/cruise_inventory/report/9359/
- Larter, R. D., King, E. C., Leat, P. T., Reading, A. M., Smellie, J. L., & Smythe, D. K. (1998). South sandwich slices reveal much about arc structure, geodynamics, and composition. *Eos, Transactions American Geophysical Union*, 79(24), 281. <https://doi.org/10.1029/98EO00207>
- Leat, P. T., Day, S. J., Tate, A. J., Martin, T. J., Owen, M. J., & Tappin, D. R. (2013). Volcanic evolution of the South Sandwich volcanic arc, South Atlantic, from multibeam bathymetry. *Journal of Volcanology and Geothermal Research*, 265, 60–77. <https://doi.org/10.1016/j.jvolgeores.2013.08.013>
- Leat, P. T., Fretwell, P. T., Tate, A. J., Larter, R. D., Martin, T. J., Smellie, J. L., et al. (2016). Bathymetry and geological setting of the South Sandwich Islands volcanic arc. *Antarctic Science*, 28(4), 293–303. <https://doi.org/10.1017/S0954102016000043>
- Leat, P. T., Livermore, R. A., Millar, I. L., & Pearce, J. A. (2000). Magma supply in back-arc spreading centre segment E2, East Scotia Ridge. *Journal of Petrology*, 41(6), 845–866. <https://doi.org/10.1093/ptrology/41.6.845>
- Leat, P. T., Pearce, J. A., Barker, P. F., Millar, I. L., Barry, T. L., & Larter, R. D. (2004). Magma genesis and mantle flow at a subducting slab edge: The South Sandwich arc-basin system. *Earth and Planetary Science Letters*, 227(1–2), 17–35. <https://doi.org/10.1016/j.epsl.2004.08.016>
- Leat, P. T., Smellie, J. L., Millar, I. L., & Larter, R. D. (2003). Magmatism in the South Sandwich arc. *Geological Society, London, Special Publications*, 219(1), 285–313. <https://doi.org/10.1144/GSL.SP.2003.219.01.14>
- Leat, P. T., Tate, A. J., Tappin, D. R., Day, S. J., & Owen, M. J. (2010). Growth and mass wasting of volcanic centers in the northern South Sandwich arc, South Atlantic, revealed by new multibeam mapping. *Marine Geology*, 275(1–4), 110–126. <https://doi.org/10.1016/j.margeo.2010.05.001>
- LeBas, M. J., Maitre, R. W. L., Streckenisen, A., & Zanettin, B. (1986). A chemical classification of volcanic rocks based on the total alkali-silica diagram. *Journal of Petrology*, 27(3), 745–750. <https://doi.org/10.1093/ptrology/27.3.745>
- Linse, K., Copley, J. T., Connelly, D. P., Larter, R. D., Pearce, D. A., Polunin, N. V. C., et al. (2019). Fauna of the Kemp Caldera and its upper bathyal hydrothermal vents (South Sandwich Arc, Antarctica). *Royal Society Open Science*, 6(11), 1–26. <https://doi.org/10.1098/rsos.191501>
- Linse, K., Römer, M., Little, C. T., Marcon, Y., & Bohrmann, G. (2022). Megabenthos habitats influenced by nearby hydrothermal activity on the Sandwich Plate, Southern Ocean. *Deep Sea Research Part II: Topical Studies in Oceanography*, 198, 105075. <https://doi.org/10.1016/j.dsr2.2022.105075>
- Lipman, P. W. (1997). Subsidence of ash-flow calderas: Relation to caldera size and magma-chamber geometry. *Bulletin of Volcanology*, 59(3), 198–218. <https://doi.org/10.1007/s004450050186>
- Livermore, R. (2003). Back-arc spreading and mantle flow in the East Scotia Sea. *Geological Society, London, Special Publications*, 219(1), 315–331. <https://doi.org/10.1144/GSL.SP.2003.219.01.15>
- Marcon, Y. (2019). NavCleaner (OFOS Edition) for processing raw Posidonia USBL datagrams. <https://doi.org/10.1594/PANGAEA.905243>
- Nielson, D. L., & Hulen, J. B. (1984). Internal geology and evolution of the Redondo dome, Valles Caldera, New Mexico. *Journal of Geophysical Research*, 89(B10), 8695. <https://doi.org/10.1029/JB089B10p08695>
- Pearce, J. A., Barker, P. F., Edwards, S. J., Parkinson, I. J., & Leat, P. T. (2000). Geochemistry and tectonic significance of peridotites from the South Sandwich arc-basin system, South Atlantic. *Contributions to Mineralogy and Petrology*, 139(1), 36–53. <https://doi.org/10.1007/s004100050572>
- Peters, C., Strauss, H., Haase, K., Bach, W., de Ronde, C. E., Kleint, C., et al. (2021). SO₂ disproportionation impacting hydrothermal sulfur cycling: Insights from multiple sulfur isotopes for hydrothermal fluids from the Tonga-Kermadec intraoceanic arc and the NE Lau Basin. *Chemical Geology*, 586, 120586. <https://doi.org/10.1016/j.chemgeo.2021.120586>
- Purser, A., Marcon, Y., Dreutter, S., Hoge, U., Sablotny, B., Hehemann, L., et al. (2019). Ocean floor observation and bathymetry system (OFOBS): A new towed camera/sonar system for deep-sea habitat surveys. *IEEE Journal of Oceanic Engineering*, 44(1), 87–99. <https://doi.org/10.1109/joe.2018.2794095>
- Riley, T. R., Carter, A., Leat, P. T., Burton-Johnson, A., Bastias, J., Spikings, R. A., et al. (2019). Geochronology and geochemistry of the northern Scotia Sea: A revised interpretation of the North and West Scotia ridge junction. *Earth and Planetary Science Letters*, 518, 136–147. <https://doi.org/10.1016/j.epsl.2019.04.031>
- Rogers, A. D. (2010). The expedition JC42 of the RRS James Cook in 2010. *Chemosynthetic Ecosystems of the Southern Ocean (CHESSO)*. Retrieved from https://bodc.ac.uk/resources/inventories/cruise_inventory/reports/jc042.pdf
- Rogers, A. D., Tyler, P. A., Connelly, D. P., Copley, J. T., James, R., Larter, R. D., et al. (2012). The discovery of new deep-sea hydrothermal vent communities in the Southern Ocean and implications for biogeography. *PLoS Biology*, 10(1), e1001234. <https://doi.org/10.1371/journal.pbio.1001234>
- Seewald, J. S., Reeves, E. P., Bach, W., Saccocia, P. J., Craddock, P. R., Shanks, W. C., et al. (2015). Submarine venting of magmatic volatiles in the Eastern Manus Basin, Papua New Guinea. *Geochimica et Cosmochimica Acta*, 163, 178–199. <https://doi.org/10.1016/j.gca.2015.04.023>
- Smith, R. L., & Bailey, R. A. (1968). Resurgent Cauldrons. In *Studies in volcanology* (Vol. 116, pp. 613–662). Geological Society of America (Geological Society of America Memoirs). <https://doi.org/10.1130/MEM116-p613>
- Tyler, P. A. (2011). The expedition JC55 of the RRS James Cook in 2011. Bransfield Strait, the East Scotia Ridge and the Kemp Seamount Calderas. *Cruise 3 of the NERC Consortium Grant 'Chemosynthetically-driven ecosystems in the Southern Ocean: Ecology and Biogeography' (ChEsSo)*. Retrieved from https://bodc.ac.uk/resources/inventories/cruise_inventory/reports/jc055.pdf
- Vermeesch, P., & Pease, V. (2021). A genetic classification of the tholeiitic and calc-alkaline magma series. *Geochemical Perspectives Letters*, 19, 1–6. <https://doi.org/10.7185/geochemlet.2125>

- Walker, S. L., Baker, E. T., Resing, J. A., Nakamura, K., & McLain, P. D. (2007). A new tool for detecting hydrothermal plumes: An ORP sensor for the PMEL MAPR. In *AGU Fall Meeting Abstracts* (pp. V21D-0753).
- Wintersteller, P., Bohrmann, G., Gaide, S., Kürzinger, V., Lichtschlag, A., Little, C. T. S., et al. (2023). Multibeam bathymetry raw data (Atlas Hydrosweep DS 3 echo sounder entire dataset) of RV POLARSTERN during cruise PS119 [Dataset]. Alfred Wegener Institute, Helmholtz Centre for Polar and Marine Research, Bremerhaven, PANGAEA (in review). <https://doi.org/10.1594/PANGAEA.916116>